Study of Film Formation From PS Latex/TiO_2 Nanocomposites; Effect of Latex Size and TiO_2 Content

Şaziye Uğur,[1] M. Selin Sunay,[2] Önder Pekcan[3]
[1]*Department of Physics, Istanbul Technical University, Maslak 34469, Istanbul, Turkey*

[2]*Faculty of Science and Letters, Piri Reis University, Tuzla 34940, Istanbul, Turkey*

[3]*Kadir Has University, Cibali 34320, Istanbul, Turkey*

In this work, we investigated the film formation from polystyrene (PS) latex/TiO_2 nanocomposites using the steady state fluorescence (SSF) and UV–vis (UVV) techniques depending on PS particle size and TiO_2 content. The structural properties of films were characterized by scanning electron microscope (SEM). The films were prepared from pyrene (P)-labeled PS particles (SmPS:203 nm; LgPS:382 nm) by covering them with different layers of TiO_2 by dip-coating method and then annealed at elevated temperatures. Two film series (SmPS/TiO_2 and LgPS/TiO_2) were prepared and seven different films were studied in various TiO_2 contents for each series. Scattered (I_{sc}), fluorescence (I_P), and transmitted (I_{tr}) light intensities were measured after each annealing step to monitor the stages of film formation. Results showed that, SmPS/TiO_2 films undergo complete film formation independent of TiO_2 content. However, no film formation occurs above a certain TiO_2 content in LgPS/TiO_2 films. SEM images showed that SmPS/TiO_2 films have highly well-ordered microporous structures with increasing TiO_2 content after extraction of PS polymer whereas LgPS/TiO2 composites show no porous structure for high TiO_2 content. Our experiments also showed that porous TiO_2 films with different sizes could be successfully prepared using this technique. POLYM. COMPOS., 35:2376–2389, 2014. © 2014 Society of Plastics Engineers

INTRODUCTION

Film formation from soft (low-T_g) and hard (high-T_g) latex dispersions can occur in several stages. In both cases, the first stage corresponds to the wet initial stage. Evaporation of solvent leads to second stage in which the particles form a close packed array, here if the particles are soft they are deformed to polyhedrons. Hard latex however stays undeformed at this stage. Annealing of soft particles causes diffusion across particle–particle boundaries which lead to a homogeneous continuous material. In the annealing of hard latex system, however, deformation of particles first leads to void closure [1–4] and then after the voids disappear diffusion across particle–particle boundaries starts, i.e. the mechanical properties of hard latex films evolve during annealing; after all solvent has evaporated and all voids have disappeared. Transmission electron microscopy (TEM) has been the most common technique used to investigate the structure of the dried films [5, 6]. Pattern of hexagons, consistent with face centered cubic packing, are usually observed in highly ordered films. When these films are annealed, complete disappearance of structure is sometimes observed, which is consistent with extensive polymer interdiffusion. Freeze fracture TEM (FFTEM) has been used to study the structure of dried latex films [7]. Small angle neutron scattering (SANS) has been used to study latex film formation at molecular level. Extensive studies using SANS have been performed by Sperling and co-workers [8] on compression-molded polystyrene film. Direct-nonradiative energy transfer (DET) method has been employed to investigate the film formation process from dye-labeled hard [9] and soft [10, 11] polymeric particles. The steady state fluorescence technique combined with DET has been used to examine healing and interdiffusion processes in the dye labeled poly(methyl methacrylate) (PMMA) latex systems [12–14]. Recently UV–Vis technique was used to study film formation from PMMA and polystyrene (PS) particles [15, 16] where the transmitted light intensity was monitored during film formation process.

As a result of worldwide theoretical and experimental efforts, a very good understanding of the mechanisms of latex film formation has been achieved [1–16].

Correspondence to: Şaziye Uğur; e-mail: saziye@itu.edu.tr
DOI 10.1002/pc.22905
Published online in Wiley Online Library (wileyonlinelibrary.com).

This understanding of latex film formation can now be exploited to underpin the processing of new types of coatings and development of new materials. The blending of latex particles and inorganic nanoparticles provides a facile means of ensuring dispersion at the nanometer scale in composite coatings. In last decade, there has been growing interest on producing new materials by filling polymers with inorganic natural and/or synthetic compounds. These composite materials posses high heat resistance, mechanical strength and impact resistance or present weak electrical conductivity and low permeability for gases like oxygen or water vapor. Since the inorganic particles display rather macroscopic dimensions and since there is mostly no interaction between the two mixed components at the interface between the two partners, the resulting composite materials can be seen as filled polymers. In general processing and structural development studies are coupled with investigations of coating properties including optical, electrical, and mechanical properties [17–19]. Some efforts have been made to construct microstructure and properties of coatings with composite ceramic–polymer microstructures, where the emphasis in composites in which a ceramic phase forms a connected network in a polymer matrix. Processing and microstructure development of ceramic and polymer coating prepared by depositing a solution or dispersion have been of interest in last few years [20, 21]. Colloidal ceramics, sol–gel derived ceramics and polymers have been studied as coating systems.

Organization of monodispersed colloidal particles like latex and silica microspheres into higher-order microstructures is attracting growing interest [22, 23], since it provides unique structures suitable for various advanced devices and functional materials such as photonic crystals [24] and porous polymers [25]. Colloidal crystals consisting of three-dimensional ordered arrays of monodispersed spheres, represent novel templates for the preparation of highly ordered macroporous inorganic solids, exhibiting precisely controlled pore sizes and highly ordered three-dimensional porous structures. This macroscale templating approach typically consists of three steps. First, the interstitial voids of the monodisperse sphere arrays are filled with precursors of various classes of materials, such as ceramics, semiconductors, metals, monomers, etc. In the second step, the precursors condense and form a solid framework around the spheres. Finally, the spheres are removed by either calcination or solvent extraction. Therefore, arrangements formed by latex microspheres have been extensively used as a target on which to template advanced materials. Ordered arrays of polymer (e.g., polystyrene or poly(methyl methacrylate) or silica nanospheres have been extensively studied in recent years for photonic crystal applications [26–30]. Such systems can be used as the "host" for chemically or electrochemically immobilizing semiconductor particles. Thus, the pores and voids of the ordered matrix can be filled with a metal, semiconductor, or both, which act as the "guest" material. The guest follows the symmetry layout of the voids or pores in the host matrix by self-organization, resulting in the formation of a three-dimensional array nanoarchitecture. Importantly, the macroporous films retain the periodicity of the templates and exhibit strong photonic band-gaps that can be tuned by varying the template diameter. Photonic crystals (i.e., spatially periodic structures of dielectric materials with different refractive indices) have been extensively investigated worldwide. Because the lattice constant of photonic crystals is in the visible or infrared wavelength range, they can control the propagation of photons in a way similar to the way a semiconductor does for electrons. Many studies have been carried out to predict and produce the 3D complete photonic band gap structures because of their wide potential applications in optics [31]. Recently, they have attracted renewed interest, mainly because they provide a much simpler, faster, and cheaper approach than complex semiconductor nanolithography techniques to create three-dimensional photonic crystals working in the optical wavelength range [32–34].

In the present study, we investigated the influence of the TiO_2 content and PS particle size on film formation process and morphology of the PS/TiO_2 composite films. For this purpose, two different PS particles with the same molecular weight but different size (SmPS: 203 nm and LgPS:382 nm) were examined. PS/TiO_2 films were prepared by drying the LgPS and SmPS suspensions on glass substrates and covering them with various layers of TiO_2 by dip-coating method. Film formation process of these films were studied with annealing them in the temperature range of 100 to 280°C for 10 min and monitoring the scattered light intensity (I_{sc}), fluorescence intensity (I_P), and transmitted light intensity (I_{tr}) changes. Film morphologies were examined with scanning electron microscope (SEM). After the film formation process completed, PS polymer was extracted with toluene to produce microporous TiO_2 films. The surface morphology of the films was found to vary with the particle size of PS latex spheres and TiO_2 content. Although TiO_2 content, film thickness and molecular weight of PS were the same in both series, SmPS/TiO_2 films presented complete film formation for all TiO_2 content while film formation occurred in LgPS/TiO_2 films only above a certain TiO_2 content. SEM images reveal that for both series of composites films, porous level or structure is also affected. After extraction of the PS polymer, the PS/TiO_2 composite containing 203 nm PS particles, exhibits a quite similar highly ordered porous structure with increasing TiO_2 content whereas composites containing 382 nm PS particles show no porous structure for high TiO_2 content. In this respect the large particles (LgPS) behave differently from the small ones (SmPS). The resulting highly structured ceramics could have applications in areas ranging from quantum electronics to photocatalysis to battery materials.

EXPERIMENTAL

Materials

Synthesis of Polystyrene (Latex) Spheres. In this study, we used two types of PS latex with different diameters. The latex samples are composed of pyrene (P) labeled polystyrene. Fluorescent PS latexes were produced via emulsion polymerization process [35]. The polymerization was performed batch-wisely using a thermostatted reactor equipped with a condenser, thermocouple, mechanical stirring paddle and nitrogen inlet. Water (50 ml), Styrene monomer (3 g; 99% pure from Janssen) and 0.014 g of fluorescent 1-Pyrenylmethyl methacrylate (PolyFluor® 394) were first mixed in the polymerization reactor where the temperature was kept constant (at 70°C). The water soluble radical initiator potassium persulfate (KPS) (1.6% wt/wt over styrene) dissolved in small amount of water (2 ml) was then introduced in order to induce styrene polymerization. Different surfactant sodium dodecyl sulfate (SDS) concentrations (0.03 and 0.12% wt/vol) were added in the polymerization recipe to change the particle size keeping all other experimental conditions the same. The polymerization was conducted under 400 rpm agitation during 12 h under nitrogen atmosphere at 70°C. The particle size was measured using Malven Instrument NanoZS. The mean diameter of these particles is 203 nm (SmPS) and 382 nm (LgPS). The weight-average molecular weights (M_w) of individual PS chains (M_w) were measured by gel permeation chromatography (GPC) and found for both SmPS and LgPS as 90×10^3 g/mol. The particle size of the polystyrene latex was decreased with increasing the concentration of SDS but its molecular weight remained almost unchanged with increasing SDS concentration. Glass transition temperature (T_g) of the PS latexes were determined using differential scanning calorimeter (DSC) and found to be around 105°C. Table 1 provides some characteristics of the two parent latex dispersions used in making the composite films.

TiO_2 Solution. TiO_2 sol was prepared at room temperature in the following way: 1.2 ml titanium(IV) butoxide was injected slowly in 15 ml ethanol. A few drop of acetic acid was added and stirred for half an hour. Later, 10 ml ethanol was added to this mixture and stirred for 1 h.

Preparation of PS/TiO_2 Films

Firstly, the glass substrates (0.8 cm × 2.5 cm) were cleaned ultrasonically in acetone and deionized water, respectively. LgPS and SmPS aques suspensions were dropped on clean glass substrates by casting method and dried at room temperature. Upon slow drying at room temperature, powder LgPS and SmPS films were produced. The film thickness of the both powder films was determined to be 5 μm in average. As our aim is to study the particle size effect of PS latex and TiO_2 content on film formation behavior of PS/TiO_2 composites, we prepared two series of films; series 1: LgPS and TiO_2 (LgPS/TiO_2) and series 2: SmPS and TiO_2 (SmPS/TiO_2). We will refer to the particle types using the abbreviations shown in Table 1 and in parentheses above. TiO_2 sol was filled into the PS templates by dip-coating method. The LgPS and SmPS covered glass substrates are settled vertically into the TiO_2 sol for two minutes, drawn out and dried at 100°C for 10 min. Here the TiO_2 content in the films could be adjusted by dipping cycle and therefore, to investigate effect of TiO_2 content the consecutive dipping was performed. When the templates were immersed into the TiO_2 sol, the TiO_2 precursor could permeate the close-packed arrays of PS by capillary force and form a solid skeleton around the PS spheres. Seven different films for each series of films were produced with 0, 1, 3, 5, 8, 10, and 15 layers (dipping cycle) of TiO_2. In order to study the film formation behavior of PS/TiO_2 composites, the produced films were separately annealed above T_g of PS, 105°C for 10 min at temperatures ranging from 100 to 280°C. The temperature was maintained within ±2°C during annealing. After each annealing step, films were removed from the oven and cooled down to room temperature.

Finally, after film formation process of PS/TiO_2 composites completed, the PS phase was dissolved away in toluene for 24 h, leaving the TiO_2 film with the nanoholes in it.

TABLE 1. Properties of the neat latexes.

Latex sample	$M_w \times 10^3$ (g mol^{-1})	PI (M^w/M^n)	Particle size (nm)	SDS (%) (wt/vol)
SmPS	90	3.5	203	0.12
LgPS	90	4.3	382	0.03

Methods

Fluorescence Measurements. After annealing, each sample was placed in the solid surface accessory of a Perkin-Elmer Model LS-50 fluorescence spectrometer. Pyrene was excited at 345 nm and scattered and fluorescence emission spectra were detected between 300 and 500 nm. All measurements were carried out in the front-face position at room temperature. Slit widths were kept at 8 nm during all SSF measurements.

Photon Transmission Measurements. Photon transmission experiments were carried out using Variant Carry-100 BioUV-Visible (UVV) scanning spectrometer. The transmittances of the films were detected at 500 nm. A glass plate was used as a standard for all UVV experiments, and measurements were carried out at room temperature after each annealing processes.

Scanning Electron Microscopy (SEM) Measurements. Scanning electron micrographs of the PS/TiO_2 films were taken at 10 to 20 kV in a JEOL 6335F microscope.

 DOI 10.1002/pc

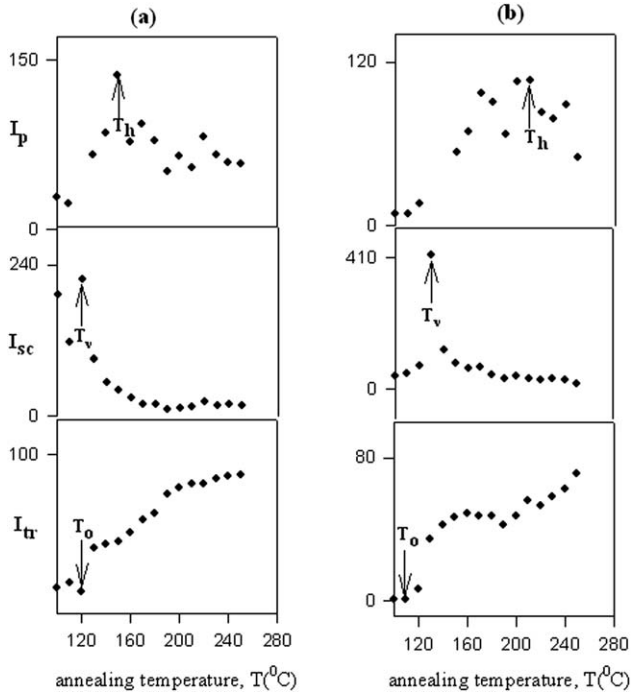

FIG. 1. Plot of I_{tr}, I_{sc}, and I_P intensities of pure a) SmPS and b) LgPS films versus annealing temperature, T. Here T_0 is the minimum film formation temperature, T_v is the void closure temperature, and T_h is the healing temperature.

A thin film of gold (10 nm) was sputtered onto the surface of samples using a Hummer-600 sputtering system to help image the PS/TiO_2 films against the glass background.

RESULTS AND DISCUSSIONS

Figure 1a and b show transmitted (I_{tr}), scattered (I_{sc}), and fluorescence (I_P) light intensities versus annealing temperatures for both pure SmPS and LgPS films with no TiO_2 content, respectively. Upon annealing the transmitted light intensity, I_{tr}, started to increase above a certain onset temperature, called the minimum film formation temperature T_0, for all film samples. Scattered light intensity showed a sharp increase at the single temperature named as the void closure temperature, T_v. Here we have to mention that I_{sc} is scattered from below the surface as well as from the surface of the latex film; however, I_{tr} goes through the film all the way. Fluorescence intensity I_P first, increase, reach a maximum, and then decrease with increasing annealing temperature [36–40]. The temperature where I_P reaches the maximum is called the healing temperature, T_h. The increase in I_{tr} above T_0 can be explained by evaluation of the transparency of the PS films upon annealing. Most probably, increased I_{tr} corresponds to the void closure process [37]; i.e., polystyrene start to flow upon annealing and voids between particles can be filled. Since higher I_{tr} corresponds to higher clarity of the composite, then increase in I_{tr} predicts that microstructure of these films change considerably by annealing them, i.e. the transparency of these films evolve upon annealing. PS starts to flow due to annealing, and voids between particles can be filled due to the viscous flow. Further annealing at higher temperature causes healing and interdiffusion processes [37–40], resulting in a more transparent film.

The sharp increase in I_{sc} occurs at T_v, which overlaps the inflection point on the I_{tr} curve. Below T_v, light scatters isotropically because of the rough surface of the PS films. Annealing of the film at T_v creates a flat surface on the film, which acts like a mirror. As a result, light is reflected to the photomultiplier detector of the spectrometer. Further annealing makes the PS film totally transparent to light and I_{sc} drops to its minimum. On the other hand, the increase in I_P above T_0 presumably corresponds to the void closure process up to the T_h point where the healing process takes place. Decrease in I_P above T_h can be understood by interdiffusion processes between polymer chains [41, 42].

I_P, I_{sc}, and I_{tr} curves of SmPS/TiO_2 and LgPS/TiO_2 composite films versus annealing temperature for various TiO_2 layer content are also shown in Figs. 2 and 3, respectively. It is clear that all curves of SmPS/TiO_2 films shows similar behaviors with the pure SmPS film in Fig. 1a. This shows that SmPS/TiO_2 films undergo complete film formation process independent of TiO_2. However, LgPS/TiO_2 series accomplished film formation process up to five TiO_2 layer content, above this content no film formation process occurs. The behavior of T_0, T_v, and T_h support these findings. Minimum film formation (T_0), void closure (T_v), and healing (T_h) temperatures are important characteristic related to the film formation properties of latexes. T_0 is often used to indicate the

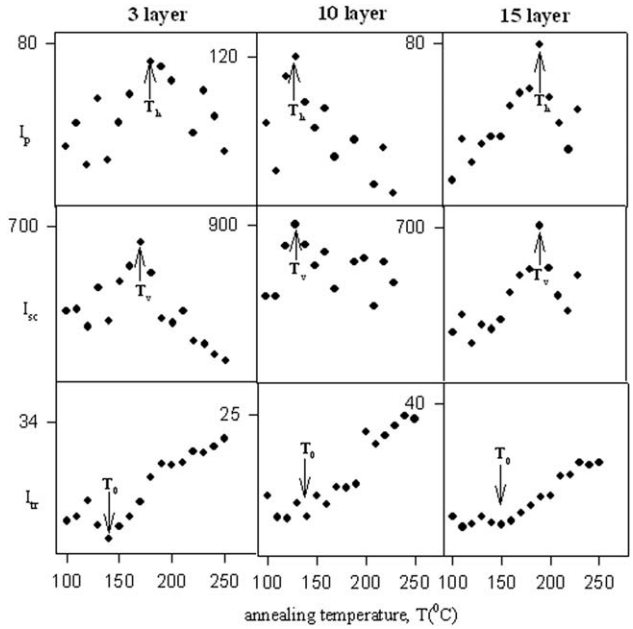

FIG. 2. Plot of I_{tr}, I_{sc}, and I_P intensities versus annealing temperature, T for SmPS/TiO_2 composite films for various TiO_2 layer. Numbers on each curve shows TiO_2 layer.

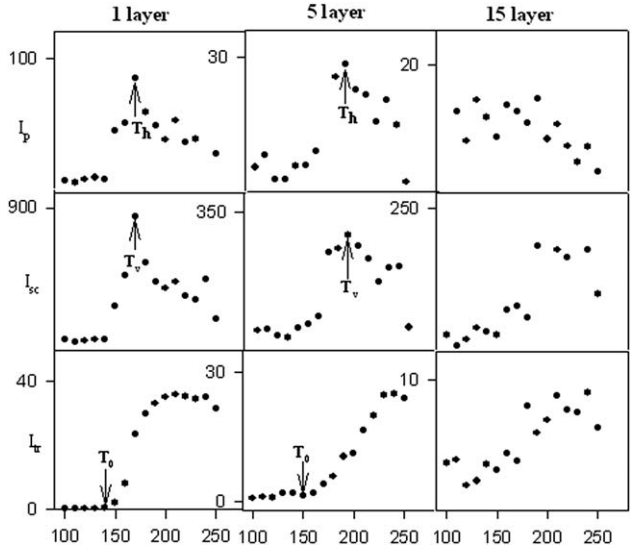

FIG. 3. Plot of I_{tr}, I_{sc}, and I_P intensities versus annealing temperature, T for LgPS/TiO_2 composite films for various TiO_2 layer. Numbers on each curve shows TiO_2 layer.

lowest possible temperature for particle deformation sufficient to decrease interstitial void diameters to sizes well below the wavelength of light [43]. Below this critical temperature, the dry latex is opaque and powdery. However, at and/or above this temperature, a latex cast film becomes continuous and clear film [44]. Therefore, T_0 has been considered in this study as the temperature above which the I_{tr} starts to increase. Here T_v is the lowest temperature at which I_{sc} become highest and defined as the maxima of the I_{sc} curve. Here T_v is the minimum temperature at which I_{sc} become highest. The healing temperature (T_h) is the minimum temperature at which the latex film becomes continuous and free of voids. The healing point indicates the onset of the particle–particle adhesion [44]. Here, T_h is defined as the maxima of the I_P curves versus temperature. T_0, T_v, and T_h, temperatures measured for two series are reported in Table 2. From Table 2, it should be noticed that T_0 and T_v values increase with increasing TiO_2 content. This behavior of T_0 and T_v clearly indicates that the existence of TiO_2 delays the latex film formation process. However, healing processes are not affected by the presence of TiO_2, which is not surprising. As a result, film formation of PS latexes was strongly influenced by both the TiO_2 content and PS particle size.

On the other hand, Fig. 4 presents the plots of the maximum values of I_{tr}, $(I_{tr})_m$ at 250°C versus number of TiO_2 layers for both series. It is seen that as the number of TiO_2 layer is increased, $(I_{tr})_m$ shows a dramatic decrease, indicating that low transparency occurs at higher TiO_2 content for both series. This indicates that increase of TiO_2 content increases the interface scattering which results in the decrease of transmission. There exist two major factors to affect the transmittance, i.e., surface scattering and (PS-PS and PS-TiO_2) boundary scattering. Before annealing, since the film contains many voids (i.e. the high number of polymer–air boundaries) most of the light is scattered at the air–polymer interface (surface scattering). Annealing the films first causes the closure of voids due to the viscous flow of PS polymer and then healing of the particle-particle boundaries. Therefore, I_{tr} increases with annealing temperature as shown in Figs. 1 to 3. After the film formation process is completed (disappearance of voids), scattering takes place predominantly from the PS-TiO_2 boundaries. As the TiO_2 content increases, the cluster size increases gradually and the screening performance of TiO_2 particles in the visible region was enhanced to result in the declined transmittance.

The behavior of I_P and I_{tr} during annealing is schematically presented in Fig. 5 where the behavior of SmPS/TiO_2 (Fig. 5; I) and LgPS/TiO_2 up to five layers of TiO_2 (Fig. 5; II) composite films during annealing are presented [39, 40]. In Fig. 5a (I,II), film posses many voids, which results in short mean-free and optical paths of a photon yielding very low I_P and I_{tr}. Figure 5b (I,II) shows a film in which interparticle voids disappear due to annealing, which gives rise to a long mean free and optical path in the film. At this stage, I_P and I_{tr} reach its maximum values. Finally, Fig. 5c (I,II) presents almost transparent film with no voids but some TiO_2 background. At this stage, film has low I_P but high I_{tr} because the mean free path is very long but the optical path is short.

TABLE 2. Minimum film formation (T_0), void closure (T_v), and healing (T_h) temperatures for two sets of films.

	SmPS/TiO_2			LgPS/TiO_2		
TiO_2 layer	T_0 (°C)	T_v (°C)	T_h (°C)	T_0 (°C)	T_v (°C)	T_h (°C)
0	120	120	150	120	130	190
1	130	150	160	140	170	170
3	140	170	170	160	210	200
5	150	170	170	160	190	180
8	160	170	170	–	–	–
10	140	130	130	–	–	–
15	150	190	190	–	–	–

T_0, minimum film formation temperature; T_v, void closure temperature; T, healing temperature.

 DOI 10.1002/pc

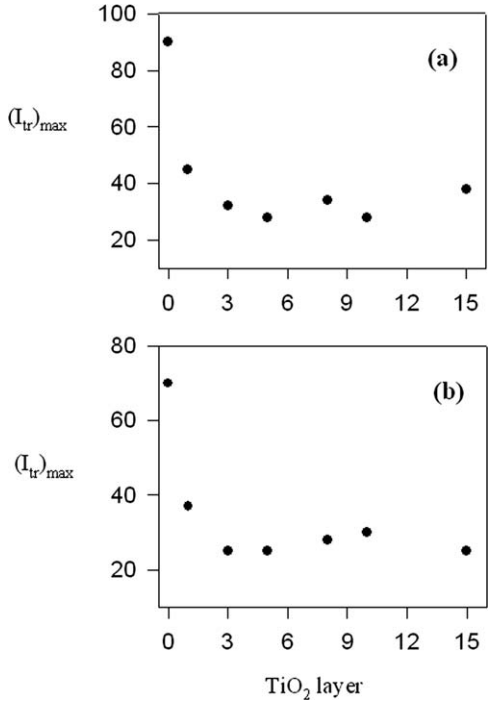

FIG. 4. Plot of the maxima of transmitted light intensities, $(I_{tr})_m$ from Figs. 1 to 3 versus TiO_2 layers for a) SmPS/TiO_2 and b) LgPS/TiO_2 films.

Film Formation Mechanisms

Void Closure. In order to quantify the behavior of I_P in Figs. 1 to 3, below T_h and above T_0, a phenomenological void closure model can be introduced. Latex deformation and void closure between particles can be induced by shearing stress which is generated by surface tension of the polymer, i.e. polymer–air interfacial tension. The void closure kinetics can determine the time for optical transparency and latex film formation [45]. In order to relate the shrinkage of spherical void of radius, r, to the viscosity of the surrounding medium, η, an expression was derived and given by the following relation [45].

$$\frac{dr}{dt} = -\frac{\gamma}{2\eta}\left(\frac{1}{\rho(r)}\right) \tag{1}$$

where γ is the surface energy, t is time, and $\rho(r)$ is the relative density. It has to be noted that here the surface energy causes a decrease in void size and the term $\rho(r)$ varies with the microstructural characteristics of the material, such as the number of voids, the initial particle size and packing. *Equation 1* is similar to one that was used to explain the time dependence of the minimum film formation temperature during latex film formation [46, 47]. If the viscosity is constant in time, integration of *Eq. 1* gives the relation as

$$t = -\frac{2\eta}{\gamma}\int_{r_0}^{r}\rho(r)dr \tag{2}$$

where r_0 is the initial void radius at time $t = 0$. The dependence of the viscosity of polymer melt on temperature is affected by the overcoming of the forces of macromolecular interaction, which enables the segments of polymer chain to jump over from one equilibration position to another. This process happens at temperatures at which the free volume becomes large enough and is connected with the overcoming of the potential barrier. Frenkel–Eyring theory produces the following relation for the temperature dependence of viscosity [48, 49]

$$\eta = \frac{N_0 h}{V}\exp\left(\frac{\Delta G}{kT}\right) \tag{3}$$

where N_0 is Avogadro's number, h is Planck's constant, V is molar volume, and k is Boltzmann's constant. It is known that $\Delta G = \Delta H - T\Delta S$, so *Eq. 3* can be written as

$$\eta = A\exp\left(\frac{\Delta H}{kT}\right) \tag{4}$$

where ΔH is the activation energy of viscous flow, i.e. the amount of heat which must be given to one mole of material to create the act of a jump during viscous flow; ΔS is the entropy of activation of viscous flow. Here A represents a constant for the related parameters that do not depend on temperature. Combining *Eqs. 2* and *4*, the following useful equation is obtained

$$t = -\frac{2A}{\gamma}\exp\left(\frac{\Delta H}{kT}\right)\int_{or}^{r}\rho(r)dr \tag{5}$$

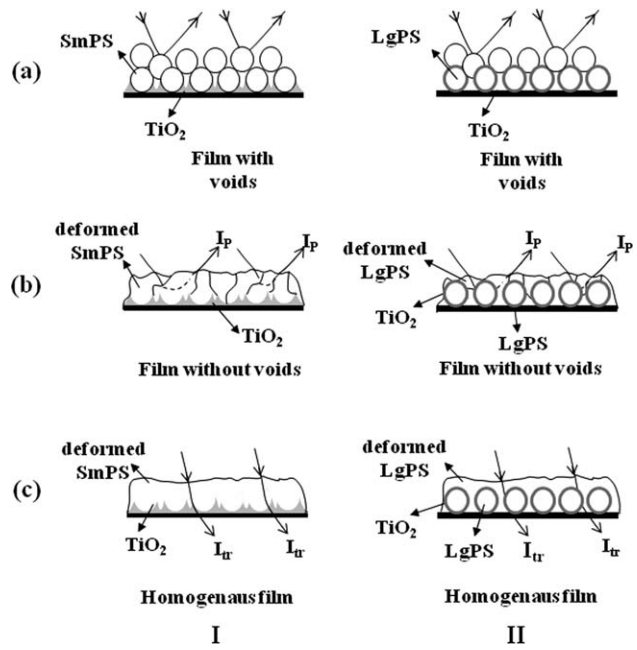

FIG. 5. Cartoon representation of (I) SmPS/TiO_2 composite films and (II) LgPS/TiO_2 composite films up to 5 layer of TiO_2 content at several annealing steps. (a) Film posses many voids that results in very low I_P and I_{tr}, (b) interparticle voids disappear due to annealing, I_P reaches its maximum value, and (c) transparent film with no voids but some Al_2O_3 background and has low I_P but high I_{tr}.

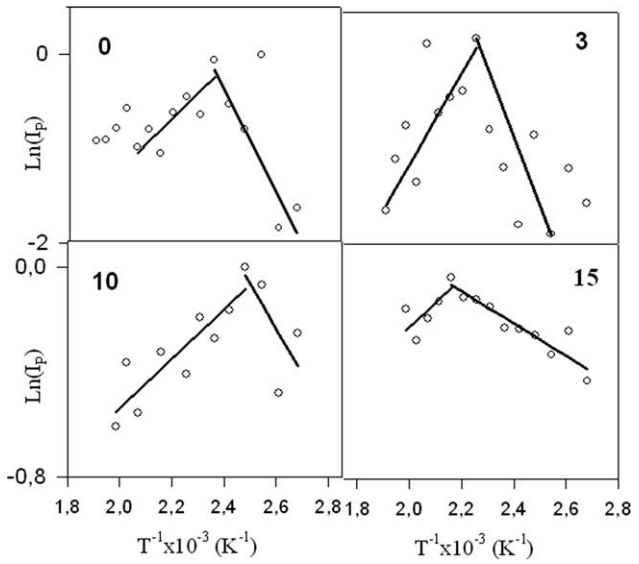

FIG. 6. The $\ln(I_P)$ versus T^{-1} plots of the data in Figs. 1a and 2 for $SmPS/TiO_2$ composite films with 0, 3, 10, and 15 layers of TiO_2. The slope of the straight lines on right and left hand side of the graph produce ΔH_P and ΔE activation energies, respectively.

In order to quantify the above results, *Eq. 5* can be employed by assuming that the interparticle voids are equal in size and the number of voids stays constant during film formation (i.e.$\rho(r) \approx r^{-3}$), Then integration of *Eq. 5* gives the relation

$$t = \frac{2AC}{\gamma} \exp\left(\frac{\Delta H}{kT}\right)\left(\frac{1}{r^2} - \frac{1}{r_0^2}\right) \tag{6}$$

where C is a constant related to relative density $\rho(r)$. As we stated before, decrease in void size (r) causes an increase in I_P. If the assumption is made that I_P is inversely proportional to the sixth power of void radius, r, then *Eq. 6* can be written as

$$t = \frac{2AC}{\gamma} \exp\left(\frac{\Delta H}{kT}\right)\left(I^{1/3}\right) \tag{7}$$

Here, r_o^{-2} is omitted from the relation since it is very small compared with r^{-2} values after void closure process is started. *Equation 7* can be solved for I_P and I_{tr} $(=I)$ to interpret the results in Figs. 1 to 4 as

$$I(T) = S(t) \exp\left(-\frac{3\Delta H}{kT}\right) \tag{8}$$

where $S(t) = (\gamma t/2AC)^3$. For a given time the logarithmic form of *Eq. 5* can be written as follows

$$LnI(T) = LnS(t) - \left(\frac{3\Delta H}{kT}\right) \tag{9}$$

As it was already argued above that, the increase in both I_P and I_{tr} originate due to the void closure process, then *Eq. 9* was applied to I_{tr} above T_0 and to I_P below T_h for all film samples in two series. Figures 6 and 7 present the Ln I_P versus T^{-1} and Figs. 8 and 9 present Ln I_{tr} versus T^{-1} plots for both film series from which ΔH_P and ΔH_{tr} activation energies were obtained. The measured ΔH_P and ΔH_{tr} activation energies are listed in Table 3. It is seen that ΔH_P values, except for pure SmPS and LgPS films, for both series do not change much by increasing the TiO_2 layer showing that the amount of heat that was required by one mole of polymeric material to accomplish a jump during viscous flow does not change by varying the TiO_2 layers on the latex films. In addition, ΔH_{tr} values of $SmPS/TiO_2$ films also do not change much while those for $LgPS/TiO_2$ series decreases with increasing TiO_2 content. It has to be noted that the measured activation energies for viscous flow process in $LgPS/TiO_2$ films were found to be different in different techniques i.e. ΔH_P values are found lower than ΔH_{tr} values. This difference most probably originates from different techniques and second one measures the film formation from the inner latexes, which requires higher energies. Moreover, since pyrenes are labeled to PS chain, it is believed that ΔH_P values are more realistic to interpret the viscous flow. On the other hand, ΔH_{tr} values were obtained

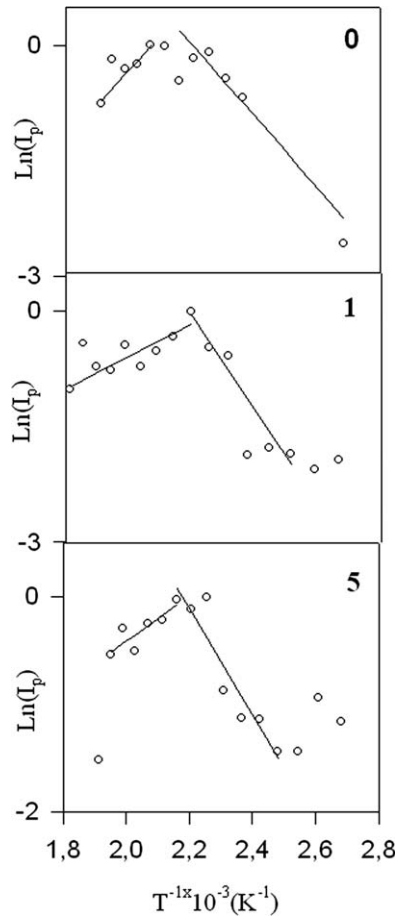

FIG. 7. The $\ln(I_P)$ versus T^{-1} plots of the data in Figs. 1b and 3 for $LgPS/TiO_2$ composite films with 0, 1, and 5 layers of TiO_2. The slope of the straight lines on right and left hand side of the graph produce ΔH_P and ΔE activation energies, respectively.

 DOI 10.1002/pc

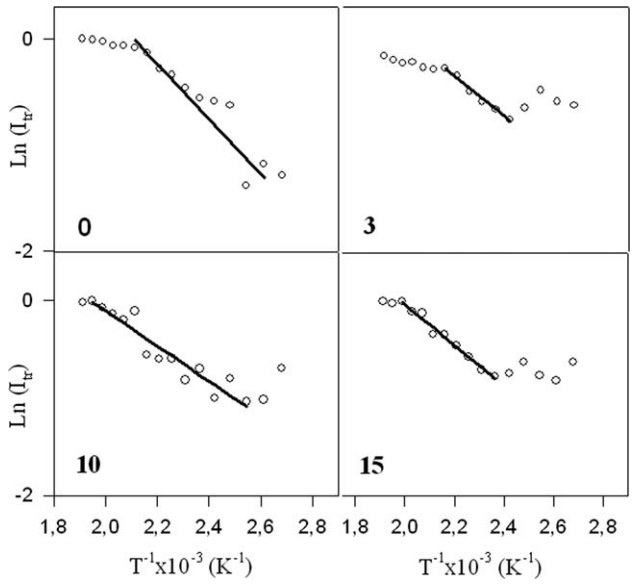

FIG. 8. The ln(I_{tr}) versus T^{-1} plots of the data in Figs. 1a and 2 for SmPS/TiO_2 composite film contains 0, 3, 10, and 15 layers of TiO_2. The slope of the straight lines produces ΔH_{tr}.

indirectly compared to ΔH_P values. Meanwhile, values for LgPS/TiO_2 series are larger than SmPS/TiO_2.

When comparing the activation energies of both series, it is seen that ΔH values of LgPS/TiO_2 series are larger than those of SmPS/TiO_2 series. This implies that the viscous flow process is significantly affected by the PS particle size. With smaller diameter (i.e., 203 nm), the SmPS particles have larger surface area or surface free energy. The driving force for film formation is proportional to the inverse of the particle size, according to the descriptions of film formation driven by capillary forces [41]. The greater curvature and higher surface area of small particles are expected to encourage film formation. The specific surface area or the total surface energy of SmPS particles (diameter 203 nm) is much larger than that of LgPS particles (diameter 382 nm). As their total surface energy is much less than that of SmPS particles, LgPS particle requires higher energy to complete viscous flow process.

Healing and Interdiffusion. The decrease in I_P was already explained in previous section, by interdiffusion of polymer chains. As the annealing temperature is increased above maxima, some part of the polymer chains may cross the junction surface and particle boundaries disappear, as a result I_P decreases due to transparency of the film. In order to quantify these results, the Prager-Tirrell (PT) model [50, 51] for the chain crossing density can be employed. These authors used de Gennes's "reptation" model to explain configurational relaxation at the polymer-polymer junction where each polymer chain is considered to be confined to a tube in which executes a random back and forth motion [52]. The total "crossing density" $\sigma(t)$ (chains per unit area) at junction surface then was calculated from the contributions $\sigma 1(t)$ due to chains still retaining some portion of their initial tubes, plus a remainder $\sigma 2(t)$ i.e. contribution comes from chains which have relaxed at least once. In terms of reduced time $\tau = 2\nu t/N^2$ the total crossing density can be written as [53]

$$\sigma(\tau)/\sigma(\infty) = 2\pi^{-1/2}\tau^{1/2} \tag{10}$$

where v and N are the diffusion coefficient and number of freely jointed segment of polymer chain [50].

In order to compare our results with the crossing density of the PT model, the temperature dependence of $\sigma(\tau)/\sigma(\infty)$ can be modeled by taking into account the following Arrhenius relation for the linear diffusion coefficient

$$v = v_o \exp(-\Delta E/kT) \tag{11}$$

Here ΔE is defined as the activation energy for backbone motion depending on the temperature interval. Combining *Eqs. 10* and *11* a useful relation is obtained as

$$\sigma(\tau)/\sigma(\infty) = R_o \exp(-\Delta E/2kT) \tag{12}$$

where $R_o = (8\nu_o t/\pi N^2)^{1/2}$ is a temperature independent coefficient. The decrease in I_P in Figs. 1 to 4 above T_h is

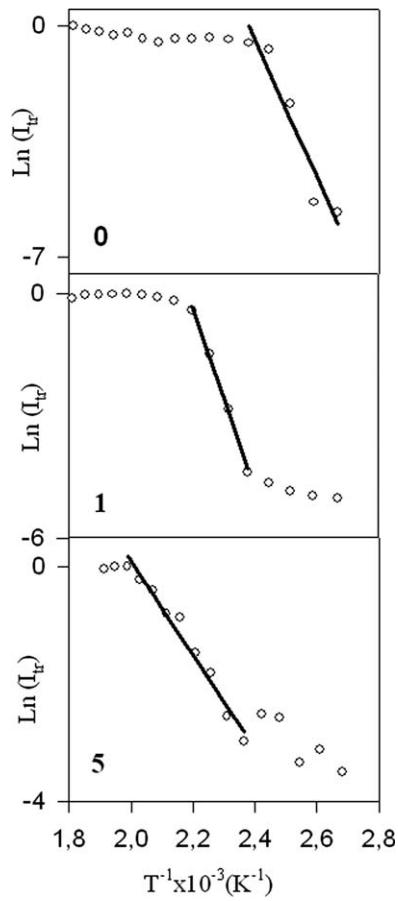

FIG. 9. The ln(I_{tr}) versus T^{-1} plots of the data in Figs. 1b and 3 for LgPS/TiO_2 composite film contains 0, 1, and 5 layers of TiO_2. The slope of the straight lines produces ΔH_{tr}.

TABLE 3. Experimentally produced activation energies for SmPS/TiO_2 and LgPS/TiO_2 films for varying numbers of TiO_2 layer.

	SmPS/TiO_2			LgPS/TiO_2		
TiO_2 layer	ΔH_P (kcal mol^{-1})	ΔH_{tr} (kcal mol^{-1})	ΔE (kcal mol^{-1})	ΔH_P (kcal mol^{-1})	ΔH_{tr} (kcal mol^{-1})	ΔE (kcal mol^{-1})
0	2.5	2.2	7.5	2.2	10.6	12.6
1	0.9	0.6	5.7	3.1	11.2	6.6
3	1.1	1.0	4.2	4.5	3.8	9.0
5	1.5	1.0	3.4	2.3	3.7	5.7
8	0.9	1.1	6.2	–	–	–
10	1.1	1.2	4.9	–	–	–
15	1.8	1.4	27.8	–	–	–

ΔH_{tr}, activation energy of viscous flow (produced from I_{tr} data); ΔH_P, activation energy of viscous flow (produced from I_P data); ΔE, activation energy of back-bone motion (produced from I_P data).

already related to the disappearance of particle-particle interface. As annealing temperature increased, more chains relaxed across the junction surface and as a result the crossing density increases. Now, it can be assumed that I_P is inversely proportional to the crossing density $\sigma(T)$ and then the phenomenological equation can be written as

$$I_P(\infty)=R_0^{-1}\exp(\Delta E/2k_BT) \quad (13)$$

The activation energy of backbone motion, ΔE is produced by least-squares fitting the data in Figs. 6 and 7 (the left hand side) to *Eq. 13* and are listed in Table 3. The ΔE value for each series decreases with increasing TiO_2 layer indicating that less energy is required to accomplish the interdiffusion process across the junction surface at high TiO_2 content. When the TiO_2 content is increased, the average number of contacts between PS particles is prevented. Therefore, the film forming ability of both LgPS and SmPS latexes in composites films is limited by TiO_2 and PS chains are not completely mixed in composite film where interpenetration is inevitably limited by TiO_2 particles. As a result, in the case of increasing TiO_2 content, interpenetration of PS chains requires higher energy to accomplish their motion due to the physical restrictions by TiO_2 particles. Furthermore, ΔE values for LgPS/TiO_2 series are larger than that of SmPS/TiO_2 series. The polymer chains contain more free volume and less interaction between segments in SmPS chains leading to higher conformational energy and less interaction of polymer chains [42, 54]. Polymer chains in the SmPS particle (diameter 203 nm) are in a highly confined state because of the spatial limitation compared to that of the random-coil state [42] in LgPS particles. This is the major reason for the SmPS particles need less energy to accomplish interdiffusion process in comparison with LgPS particles. Moreover, ΔE values are also much larger than the void closure activation energies for both series. This result is understandable because a single chain needs more energy to execute diffusion across the polymer–polymer interface than to be accomplished by the viscous flow process.

FILM MORPHOLOGY

Scanning electron microscopy (SEM) was used to characterize the morphologies of the composite films. Figures 10 to 13 show SEM images of both SmPS/TiO_2 and LgPS/TiO_2 composites films with different layers of TiO_2 after thermal treatment at 100 and 280°C for 10 min, respectively. Figures 10a and 12a show that in pure SmPS and LgPS films, particles are randomly distributed and have spherical shapes. Particles in both films are in a typically ordered close-packed array and no deformation has occurred after heat treatment at 100°C. In TiO_2 content films (Fig. 10b–d and Fig. 12b,c), PS latexes still exhibit spherical shapes but consecutive dip-coating cycle seems to lead the formation of an ordered array on a larger area. The film surface of the films became smooth by increasing the TiO_2 layer content. Here as well, no deformation of particles was found and the structure of PS colloidal templates is well preserved. This confirms that particle coalescence and film formation have not yet occurred after annealing at 100°C. However, for LgPS/TiO_2 films with 10 layer of TiO_2, a solid shell of layer and cracks are seen on the surface of the film. This shows that the interstitial voids of closely-packed LgPS microspheres are fully filled with TiO_2 and TiO_2 will fully cover the top of LgPS template.

SEM images of these films show that considerable change is occurred by annealing the films at 250°C (Fig. 12a-d and Fig. 13a–c), i.e. the microstructure of the composite film is changed and particle–particle boundaries are completely disappeared after annealing process is completed. Nevertheless, SEM image of LgPS/TiO_2 film with five TiO_2 layer in Fig. 13c shows that the replica of the LgPS particles on the film surface can not be destroyed upon annealing even at 250°C temperature. However, no further significant change in the morphology of LgPS/TiO_2 film with 10 layers of TiO_2 could be detected (Fig. 13d) indicating that LgPS latexes are highly covered by a flat top layer of TiO_2. These results are in consistent with our arguments about the film formation behavior of LgPS/TiO_2 composites. From here, both optical (I_P and I_{tr}) and SEM data suggest that

 DOI 10.1002/pc

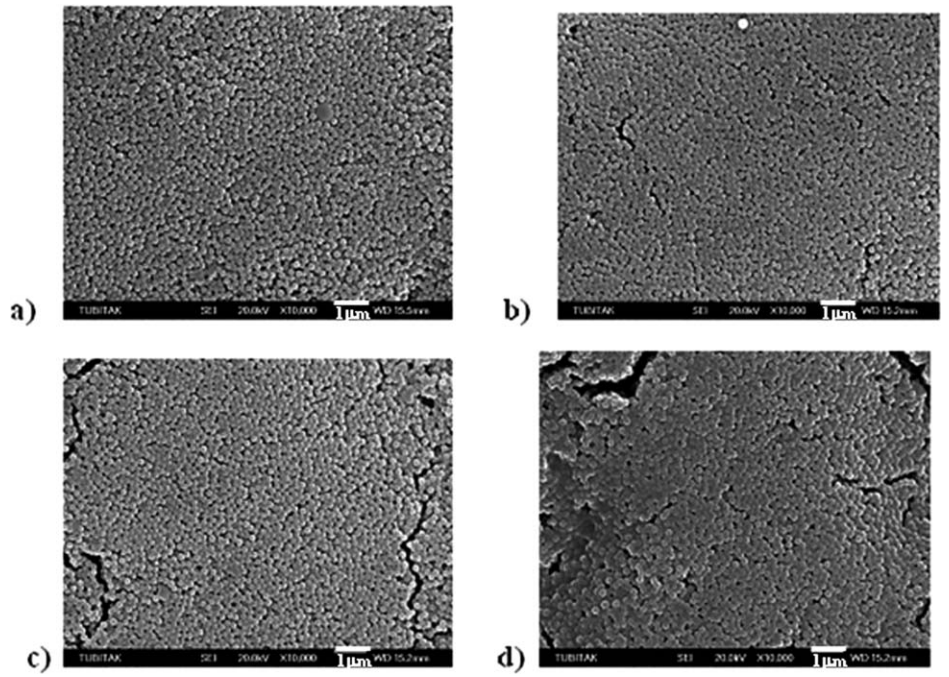

FIG. 10. SEM images of SmPS/TiO_2 composite films with a) 0, b) 1, c) 5, and d) 10 layers of TiO_2 annealed at 100°C.

10 layer of TiO_2 presents a critical content for LgPS/TiO_2 films, at or above which composite films are completely covered with TiO_2 layer which prevents film formation process of LgPS particles.

Finally, in order to determine the extent of film formation, PS polymer was removed from the composite films by extraction with toluene for 24 h. Here, toluene was used as the dissolution agent since polystyrene is very

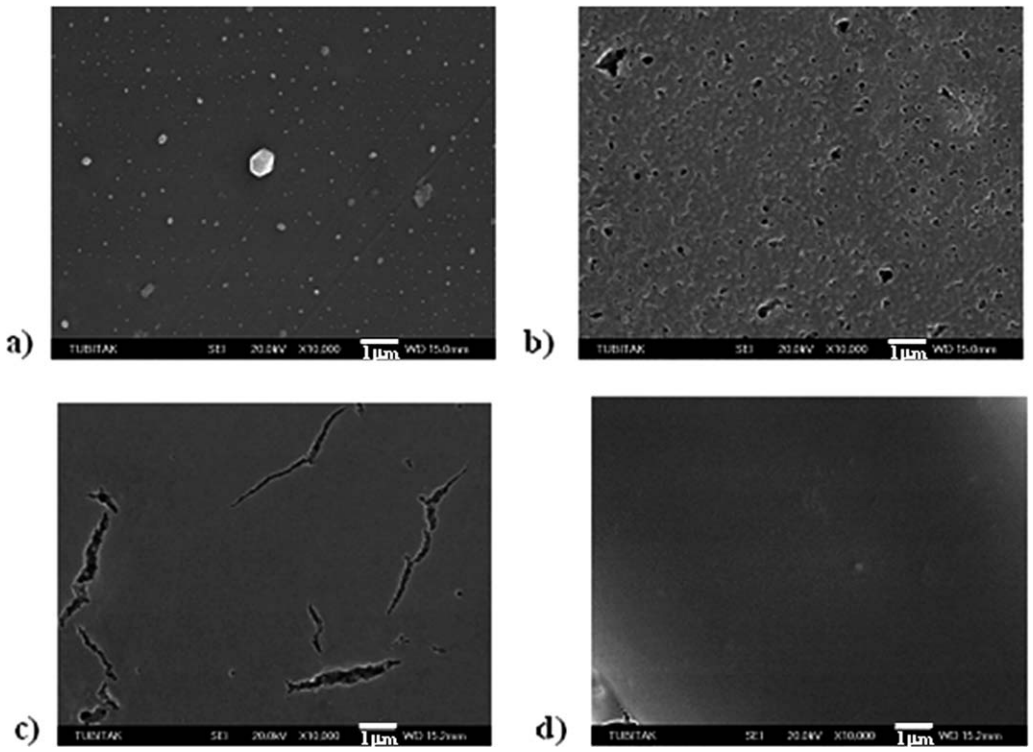

FIG. 11. SEM images of SmPS/TiO_2 composite films with a) 0, b) 1, c) 5, and d) 10 layers of TiO_2 annealed at 250°C.

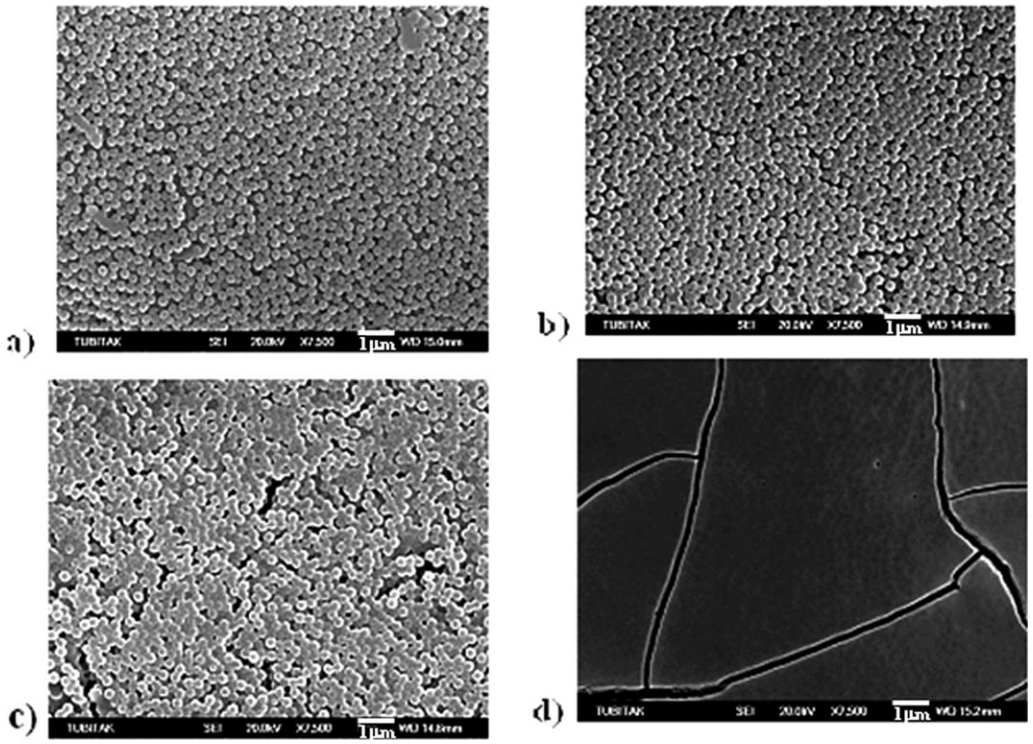

FIG. 12. SEM images of LgPS/TiO_2 composite films with a) 0, b) 1, c) 5, and d) 10 layers of TiO_2 annealed at 100°C.

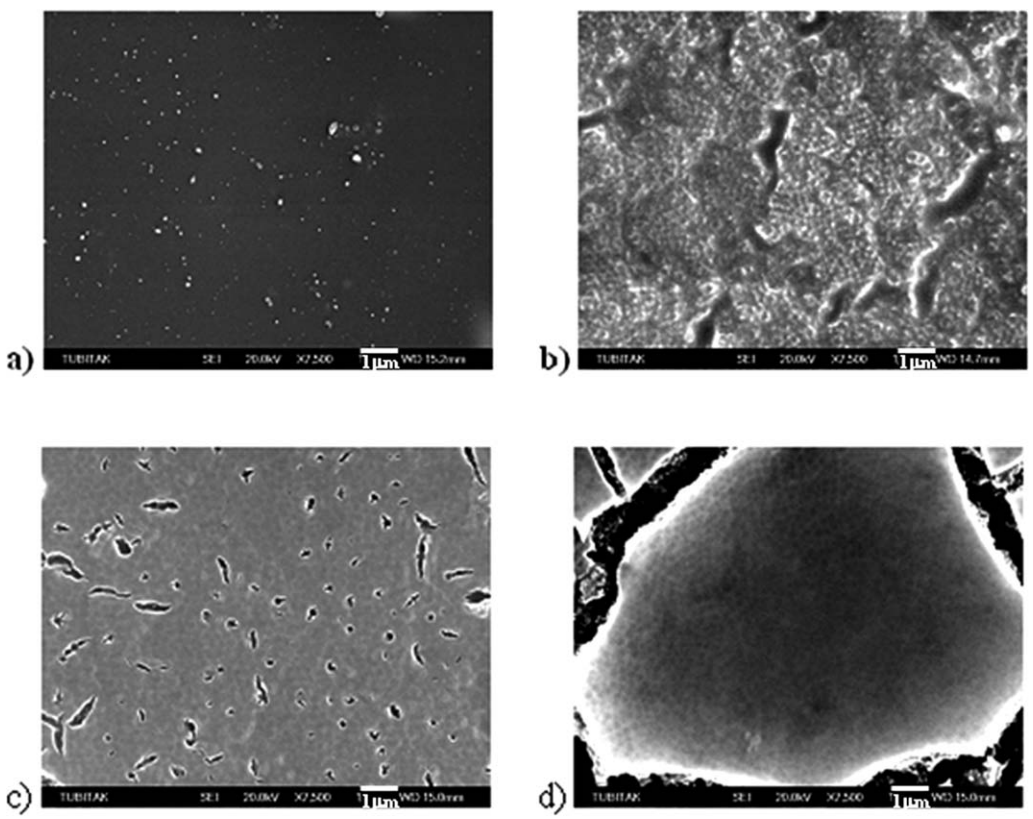

FIG. 13. SEM images of LgPS/TiO_2 composite films with a) 0, b) 1, c) 5, and d) 10 layers of TiO_2 annealed at 250°C.

 DOI 10.1002/pc

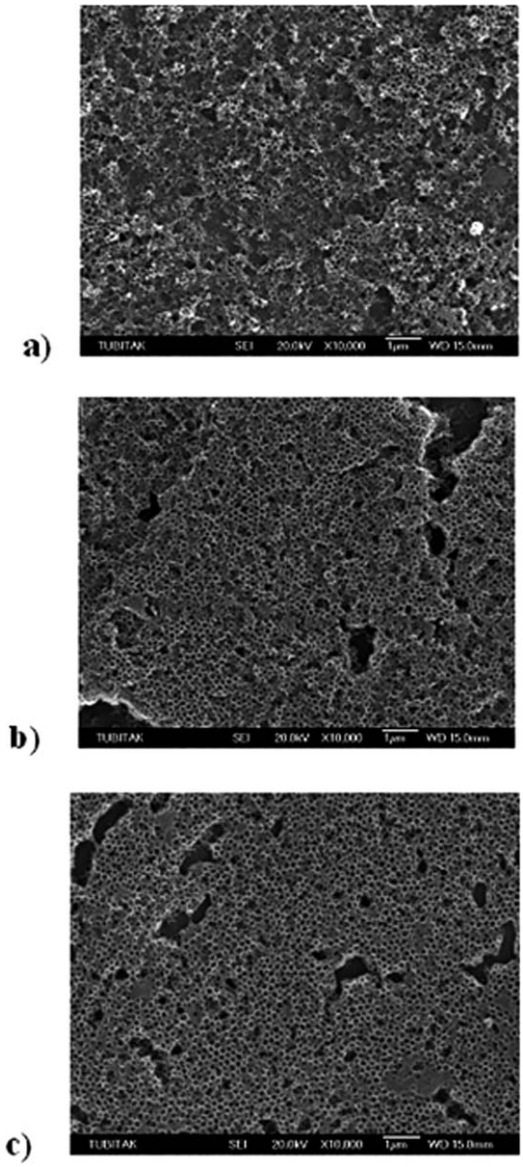

FIG. 14. SEM images of SmPS/TiO_2 films with a) 1, b) 5, and c) 10 layers of TiO_2 after extraction of PS template with toluene.

soluble [55] in this solvent and the TiO_2 films are stable. After dissolution of SmPS/TiO_2 films with 1, 5, and 10 layer of TiO_2, the microstructure of the PS particles reappeared again, as seen in Fig. 14a–c. This behavior can be explained by removal of PS from the surface of the TiO_2 covered latex particles during the dissolution process. In other words, the film formation from SmPS particles has occurred on top of the TiO_2 covered SmPS particles during annealing and, during dissolution, PS material is completely dissolved showing the microstructure of SmPS particles covered by TiO_2 layer. Cartoon presentation in Fig. 5 explains this fact, where latex film formation proceeds independent of TiO_2 content, which is placed on the bottom of the first layer of PS latexes. According to this explanation, TiO_2 structures in Fig. 5 present the monolayer replica of PS latexes. In Fig. 14a, the porous structure has primarily been formed but the inorganic wall is thin and nonuniform for one layer of TiO_2. This indicates that TiO_2 sol is easy to fully fill the interstices, but there is not enough solid content when the template is removed. However, SEM images of SmPS/TiO_2 films with 5 and 10 TiO_2 layers in Fig. 14b,c give nice hole pictures. From these images, it can also be seen that the level of order and the uniformity of inorganic wall become better with the increase of dipping cycle.

On the other hand, extraction of LgPS polymer with toluene created a porous, disordered material for the LgPS/TiO_2 film with one layer of TiO_2 (Fig. 15a). For higher TiO_2 content films in Fig. 15b,c, it can be seen that porous TiO_2 structure cannot be obtained. These films still keep their original microstructure forms and a solid shell of layer and cracks are seen still present on the surface of the films. However, the image shown in Fig. 15c reveals that three-dimensional microporous structure

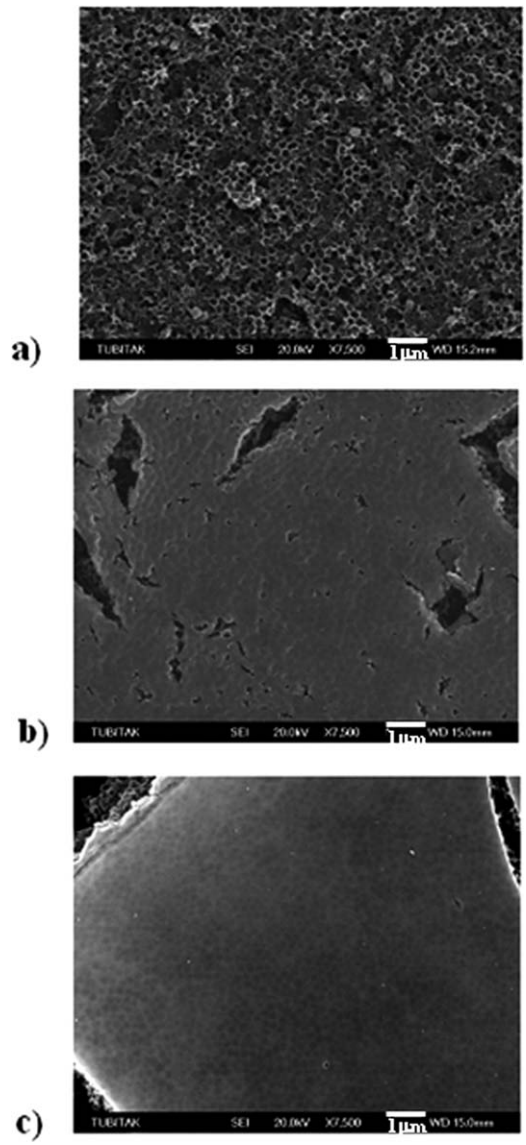

FIG. 15. SEM images of LgPS/TiO_2 films with a) 1, b) 5, and c) 10 layers of TiO_2 after extraction of PS template with toluene.

was still formed under the top TiO_2 layer demonstrating the three-dimensional nature of the templated structure. So the TiO_2 content is a key for the permeation of multilayer LgPS templates, which needs further investigation. If the TiO_2 content is more, the TiO_2 will fully cover the top of LgPS template (see Figs. 12c,d and 13b,c). Contrarily, TiO_2 cannot fully pour the interstices of LgPS and create a disordered porous structure after dissolution when the content is small (see Fig. 15a). This result suggested that the film formation of LgPS/TiO_2 nanocomposite particles was highly dependent on TiO_2 content.

In summary, we have developed a method to reliably fabricate microporous TiO_2 films on glass substrates using monodisperse SmPS (203 nm) and LgPS (382 nm) latex spheres as templates. The amount of the TiO_2 deposited was precisely controlled via the subsequence dipping cycles during the dip-coating. The highly well-ordered microporous structures were preserved after removal of PS polymer with toluene for 203 nm sized PS latex. We discovered that latex particle templating can also be used to create porous networks of numerous oxide compositions in a simple, rapid and less expensive process.

CONCLUSIONS

In conclusion this work has shown that the film formation process of PS/TiO_2 composites is highly affected by TiO_2 content and PS particle size. For SmPS/TiO_2 composite system, the classical latex film formation process can take place independent of TiO_2 content in the film. After dissolution of SmPS/TiO_2 films, the microstructure of the SmPS particles reappeared again. The microporous TiO_2 films made from the small (203 nm) latex spheres have a highly porous and regular structure with increasing TiO_2 layer retaining the SmPS template's long-range ordering. This behavior can be explained by washing of PS from the surface of the TiO_2 covered latex particles during the dissolution process. In other words, the film formation from PS particles has occurred on top of the TiO_2 covered SmPS particles during annealing and, during dissolution, PS material is completely dissolved showing the microstructure of SmPS particles covered by TiO_2 layer. On the other hand, except low TiO_2 content films, no film formation process occurred for high TiO_2 content LgPS/TiO_2 films indicating that LgPS particles are completely covered by TiO_2. Since LgPS particles were prevented from coming into contact, LgPS latexes were no longer film forming at high TiO_2 content. After dissolution, films made from large (382 nm) latex spheres gave poorly ordered porous films only for one layer of TiO_2, whereas for higher TiO_2 content no porous structure was observed. The morphological changes were found in consistent with the SSF and UVV-results for both film series.

This work also showed that, using dip-coating method which is the simplest and less expensive technique, depending on the TiO_2 content and size of the PS latex used, periodic, interconnected networks of monodisperse submicron inorganic oxide pores could be formed. These structures could potentially find applications as chromatographic support materials, solid catalysts, battery materials, thermal insulators, or photonic crystals. We anticipate that with this strategy, the synthesis of other highly ordered micromacroporous metal oxide films should also be possible. In future work, we will investigate the detailed film formation mechanism of other metal oxide/latex polymer composites and the possibility of producing the diversity of macroporous materials achievable with this technique.

ACKNOWLEDGMENTS

Önder Pekcan thanks the Turkish Academy of Sciences (TUBA) for their partial support. Dr. Sunay thank the Laboratories in Physics Department of ITU, where she has done the experimental work during her PhD studies and to prepare this article.

REFERENCES

1. P.R. Sperry, B.S. Synder, M.L. O'Dowd, and P.M. Lesko, *Langmuir*, **10**, 2619 (1994).
2. S. Mazur, "Coalescence of Polymer Particles," in *Polymer Powder Processing*, N. Rosenweig, Ed., Wiley, New York (1995).
3. J.K. Mackenzie and R. Shutlewort, *Proc. Phys. Soc*., **62**, 838 (1946).
4. J.W. Vanderhoff, *Br. Polym. J*., **2**, 161 (1970).
5. G. Kanig and H. Neff, *Colloid Polym. Sci*., **256**, 1052 (1975).
6. Y. Wang, A. Kats, D. Juhue, M.A. Winnik, R.R. Shivers, and C.J. Dinsdale, *Langmuir*, **8**, 1435 (1992).
7. B.J. Roulstone, M.C. Wilkinson, J. Hearn, and A.J. Wilson, *Polym. Int*., **24**, 87 (1991).
8. K.D. Kim, L.H. Sperling, and A. Klein, *Macromolecules*, **26** 4624 (1993).
9. Ö. Pekcan, M.A. Winnik, and M.D. Croucher, *Macromolecules*, **23** 2673 (1990).
10. Y. Wang, C.L. Zhao, and M.A. Winnik, *J. Chem. Phys*., **95**, 2143 (1991).
11. Y. Wang and M.A. Winnik, *Macromolecules*, **26** 1347 (1993).
12. Ö. Pekcan and M. Canpolat, *J. Appl. Polym. Sci*., **59**, 277 (1996).
13. Ö. Pekcan, M. Canpolat, and A. Göçmen, *Polymer*, **34**, 3319 (1993).
14. M. Canpolat and Ö. Pekcan, *J. Polym. Sci. Polym. Phys. Ed*., **34**, 691 (1996).
15. E. Arda, V. Bulmus, E. Piskin, and Ö. Pekcan, *J. Colloid Interface Sci*,. **213**, 160 (1999).
16. Ö. Pekcan and E. Arda, *Colloids Surf. A*, **153**, 537 (1999).
17. J. Sun, W.W. Gerberich, and L.F. Francis, *J. Polym. Sci. Part B Polym. Phys*., **41**, 1744 (2003).
18. L.F. Francis, A.V. McCormick, D.M. Vaessen, and J.A. Payne, *J. Mater. Sci*., **37**, 4897 (2002).

19. J.C. Grunlan, W.W. Gerberich, and L.H. Francis, *Polym. Eng. Sci*., **41**, 1947 (2001).
20. D.M. Vaessen, F.A. Ngantung, M.L.B. Palacio, L.F. Francis, and A.V. McCormick, *J. Appl. Polym. Sci*., **84**, 2784 (2002).
21. D.M. Vaessen, A.V. McCormick, and L.F. Francis, *Polymer*, **43**, 2267 (2002).
22. D. Wang and H. Mohwald, *J. Mater. Chem*., **14**, 459 (2004).
23. A.D. Dinsmore, M.F. Hsu, M.G. Nikolaides, M. Marquez, A.R. Bausch, and D.A. Weitz, *Science*, **298**, 1006 (2002).
24. E. Chomski and G.A. Ozin, *Adv. Mater*., **12**, 1071 (2000).
25. J.H. Moon, S. Kim, G.-R. Yi, Y.-H. Lee, and S.-M. Yang, *Langmuir*, **20**, 2033 (2004).
26. T. Yamasaki and T. Tsutsui, *Appl. Phys. Lett*., **72**, 1957 (1998).
27. Yu. A. Vlasov, K. Luterova, I. Pelant, B. Honerlage, and V.N. Astratov, *Appl. Phys. Lett*., **71**, 1616 (1997).
28. A.A. Zakhidov, R. H. Baughman, Z. Ighal, C. Cui, I. Khayrullin, S.O. Dantas, J. Marti, and V.G. Radchenko, *Science*, **282**, 897 (1998).
29. B.T. Holland, C.F. Blanford, and A. Stein, *Science*, **281**, 538 (1998).
30. Yu. A. Vlasov, N. Yao, and D.J. Norris, *Adv. Mater*., **11**, 165 (1999).
31. J.D. Joannopoulos, R.D. Meade, and N. Winn, "Photonic Crystals," in *Molding the Flow of Light*, Princeton University Press, N.J. Princeton (1995).
32. Y.A. Vlasov, X.Z. Bo, J.C. Sturm, and D.J. Norris, *Nature*, **414**, 289 (2001).
33. A. Blanco, A. Chomski, S. Grabtchak, M. Ibisate, S. John, S.W. Leonard, C. Lopez, F. Meseguer, H. Miguez, J.P. Mondia, G.A. Ozin, O. Toader, and H.M. van Driel, *Nature*, **405**, 437 (2000).
34. J. Wijnhoven and W.L. Vos, *Science*, **281**, 802 (1998).
35. J.S. Liu, J.F. Feng, and M.A. Winnik, *J. Chem. Phys*., **101**, 9096 (1994).
36. M. Canpolat and Ö. Pekcan, *J. Polym. Sci. Polym. Phys. Ed*., **34**, 691 (1996).
37. S. Ugur, A. Elaissari, and O. Pekcan, *J. Colloid Interface Sci*., **263**, 674 (2003).
38. S. Ugur, A. Elaissari, and O. Pekcan, *J. Coat. Technol.Res*., **1**, 305 (2004).
39. S. Ugur, S. Sunay, F. Tepehan, and O. Pekcan, *Compos. Interfaces*, **14**, 243 (2007).
40. S. Ugur, S. Sunay, A. Elaissari, F. Tepehan, and O. Pekcan, *Polym. Compos*., **27**, 651 (2006).
41. J.L. Keddie, *Mater. Sci. Eng*., **R21**, 101 (1997).
42. C. Wu, K.K. Chan, K.F. Woo, R. Qian, X. Li, L. Chen, D.H. Napper, G. Tan, and A.J. Hill, *Macromolecules*, **28**, 1592 (1995).
43. J.L. Keddie, P. Meredith, R.A.L. Jones, and A.M. Donald, *Macromolecules*, **28**, 2673 (1995).
44. S.T. Eckersley and A. Rudin, *J. Coat. Technol*., **62**, 89 (1990).
45. J.L. Keddie, P. Meredith, R.A.L. Jones and A.M. Donald, "Film Formation in Waterborne Coatings," in *ACS Symp. Ser*., Vol. **648**, T. Provder, M.A. Winnik, and M.W. Urban, Eds., American Chemical Society, Washington, DC, USA, 332 (1996).
46. G.B. Mc Kenna, "Glass formation and glassy behavior," in *Comprehensive Polymer Science*, Vol. **2**, C. Booth and C. Price, Eds., Pergamon Press, Oxford, UK (1989).
47. H. Vogel, *Phys. Z*., **22**, 645 (1925).
48. G.S. Fulcher, *J. Am. Ceram. Soc*., **8**, 339 (1925).
49. J. Frenkel, *J. Phys. USSR*, **9** 385 (1945).
50. S. Prager and M. Tirrell, *J. Chem. Phys*., **75**, 5194 (1981).
51. R.P. Wool, B.L. Yuan, and O.J. McGarel, *J. Polym. Eng. Sci*., **29**, 1340 (1989).
52. P.G. de Gennes, *J. Chem. Phys*., **76**, 3322 (1982).
53. Ö. Pekcan and E. Arda, *Colloids Surf. A*, **153**, 537 (1999).
54. X. Qu, Y. Tang, L. Chen, and X. Jin, *Chin. Sci. Bull*., **46**, 991 (2001).
55. S. Ugur and O. Pekcan, *J. Colloid Interface Sci*., **277**, 359 (2004).